

## Supplementary Information

### **Three-dimensional porous LiFePO<sub>4</sub> cathode material modified with nitrogen-doped graphene aerogel for high-power lithium ion batteries**

***Bo Wang,<sup>ab</sup> Wael Al Abdulla,<sup>c</sup> Dianlong Wang<sup>\*a</sup> and X. S. Zhao<sup>\*bd</sup>***

*<sup>a</sup> Harbin Institute of Technology, School of Chemical Engineering and Technology, Xidazhi Street, 150001 Harbin, China. Fax: 86 451 86413721; Tel: 86 451 86413751; E-mail: [wangdianlongwbhit@163.com](mailto:wangdianlongwbhit@163.com)*

*<sup>b</sup> The University of Queensland, School of Chemical Engineering, St Lucia, Brisbane, QLD 4072, Australia. Fax: 61 7 33654199; Tex: 61 7 33469997; E-mail: [george.zhao@uq.edu.au](mailto:george.zhao@uq.edu.au)*

*<sup>c</sup> The University of Queensland, Australian Institute for Bioengineering and Nanotechnology, St. Lucia, Brisbane, QLD 4072, Australia.*

*<sup>d</sup> Colloge of Chemical Science and Engineering, Qingdao University, Qingdao 207661, China.*

## Experimental

### Synthesis

The graphene oxide (GO) used in this work was synthesized from natural graphite using a modified Hummers method.<sup>1</sup> (010) facet orientated LFP NPs were prepared via a solvothermal way.<sup>2</sup> APS-modified LFP NPs were obtained by a surface modification process.<sup>3</sup> LFP@GO was fabricated according to a modified procedure as previously reported.<sup>4</sup> Briefly, 20 ml GO aqueous suspension ( $0.75 \text{ mg ml}^{-1}$ ) was slowly added into 200 ml APS-modified LFP NPs aqueous dispersion ( $0.4 \text{ mg ml}^{-1}$ ) under magnetic stirring. The LFP@GO was then obtained after centrifugation and washing with distilled water.

LFP@N-GA was prepared by hydrothermal assembly of LFP@GO and additional GO sheets in a urea aqueous solution, subsequently combining with freeze-drying and thermal treatment. In a typical process, LFP@GO was homogeneously dispersed in 13 ml urea ( $70 \text{ mg ml}^{-1}$ ) aqueous solution followed by the addition of 2 ml aqueous GO suspension ( $7.5 \text{ mg ml}^{-1}$ ), and then sealed in a 20 ml polytetrafluorethylene (Teflon)-lined autoclave. After hydrothermal treatment at  $120 \text{ }^{\circ}\text{C}$  for 3 h, the autoclave was naturally cooled to room temperature; the obtained N-doped graphene hydrogel embedded with LFP NPs was taken out and freezing dried, followed by annealing at  $600 \text{ }^{\circ}\text{C}$  for 2h in reductive (5 vol.% of hydrogen in argon) atmosphere to generate 3D LFP@N-GA. N-GA and GA were prepared by assembly of GO in a similar hydrothermal process in the presence and absence of urea, respectively.

### Characterization

X-ray diffraction (XRD) patterns were collected on a Rigaku diffractometer using Cu  $K\alpha$  radiation. Raman spectra were recorded on a Thermo-Fischer Almega dispersive Raman instrument. The instrument was fitted with 633 nm lasers. Powder samples were measured at room temperature using the microscope accessory with a 50x apertures with at least 132 scans. Fourier transform infrared spectroscopy (FTIR) spectra were collected from a Nicolet 5700 FTIR spectrometer with 64 scans at a resolution of  $4 \text{ cm}^{-1}$ . Nitrogen sorption isotherms were measured on Tristar II 3020 at the liquid nitrogen temperature. Before measurement, the sample was degassed at  $150 \text{ }^{\circ}\text{C}$  for 24 h. The specific surface area was calculated using the multipoint Brunauer-Emmett-Teller (BET) method. The pore size distribution was computed using the Barrett-Joyner-Halenda (BJH) method. Thermal gravimetric analysis (TGA) was conducted in air from room temperature up to  $800 \text{ }^{\circ}\text{C}$  at a heating rate of  $10 \text{ }^{\circ}\text{C min}^{-1}$  using a Mettler Toledo TGA/DSC1 STARe System (Mettler Toledo, USA & Switzerland). The electronic conductivity was measured at room temperature using a four-probe conductivity test metre. The morphology and microstructure were characterized using JEOL 7001, 6300 field-emission scanning electron microscope (FESEM), JEOL 1010 transmission electron microscope (TEM), and FEI Tecnai 20 high-resolution (HRTEM). Chemical compositions were analysed using the X-ray photoelectron spectroscopy (XPS, Kratos Axis ULTRA) technique incorporating a 165 mm hemispherical electron energy analyser.

## Electrochemical measurements

Before electrode fabrication, the obtained LFP@N-GA monolith was ground into powder. Then, the powder was mixed with carbon black and polyvinylidene fluoride (PVDF) in a mass ratio of 8:1:1. The mixture was pasted onto the aluminum foils and dried at 80 °C for 10 h in vacuum oven before cut into disks with diameter of 1.5 cm. The disks were further compressed at a given pressure. The N-GA electrode was prepared using the same procedure to investigate the electrochemical performance of N-GA. The bare LFP@N-GA electrode without carbon black but with the same 10 wt.% of PVDF was also prepared for comparison purpose. To investigate the influence of the loading mass on the electrochemical performance, the loading mass of each disk was controlled by using different layers of the adhesive tape to control the thickness of the coating materials. The average loading masses corresponding to 1 layer, 2 layers, 3 layers and 5 layers adhesive tape thicknesses were about 1.2, 2.1, 3.3, 5.6 mg·cm<sup>-2</sup>, respectively. Without special explanation, the electrochemical data were corresponded to 5 layer adhesive tape thicknesses (~ 100 um). The CR2032 coin-type cells were assembled in an argon-filled glove box using the prepared disks as cathode, metal lithium disks as anode, Celgard 2500 (polypropylene) as separator, and 1 M of LiPF<sub>6</sub> in ethylene carbonate (EC)/ dimethyl carbonate (DMC)/ diethyl carbonate (DEC) solvent (1:1:1 in volume) as electrolyte. The cells were charged and discharged over a potential range of 2.5-4.2 V (vs. Li/Li<sup>+</sup>) at different current rates. Note that “n C” means that the charge/discharge current is set up to achieve the nominal capacity (170 mAh·g<sup>-1</sup>) in “1/n” hours. Among the components of the prepared LFP@N-GA electrodes, we regarded LFP@N-GA as the active material, so that the specific capacities were calculated based on the total mass of LFP NPs and N-GA.

Electrochemical impedance spectroscopy (EIS) and cyclic voltammetry (CV) data were collected on an electrochemical workstation (CHI 660D or PARSTAT 2273). The CV measurement was carried out at a scanning rate of 0.1 mV·s<sup>-1</sup> between 2.5 and 4.2 V. The EIS measurement was performed over a frequency range of 100 kHz to 10 mHz with an applied amplitude of 5 mV. The parameters of the equivalent circuit were calculated and analyzed by computer simulations using the ZSimpWin software.

### S1. Morphology information of the as-prepared LFP NPs

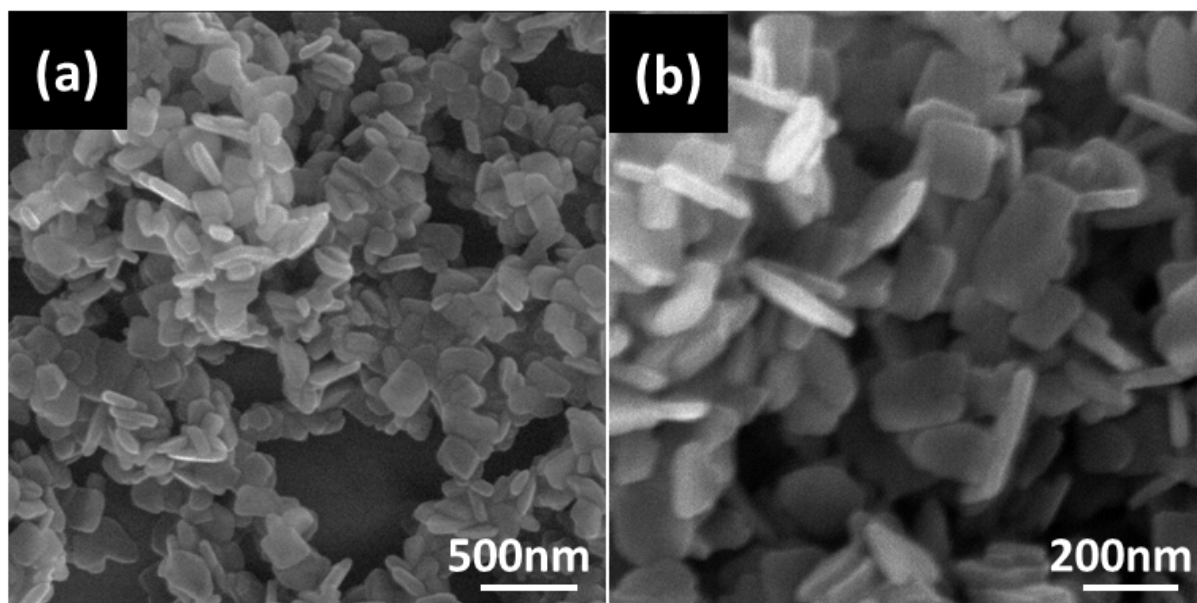


**Fig. S1†** (a) Low- and (b) high-magnification SEM images of the as-prepared LFP NPs, showing the length, width and thickness of the LFP NPs are ranged of 150-200 nm, 70-100 nm and 30-40 nm, respectively, as well as the severe agglomeration between LFP NPs.

## S2. Morphology information of LFP@GO

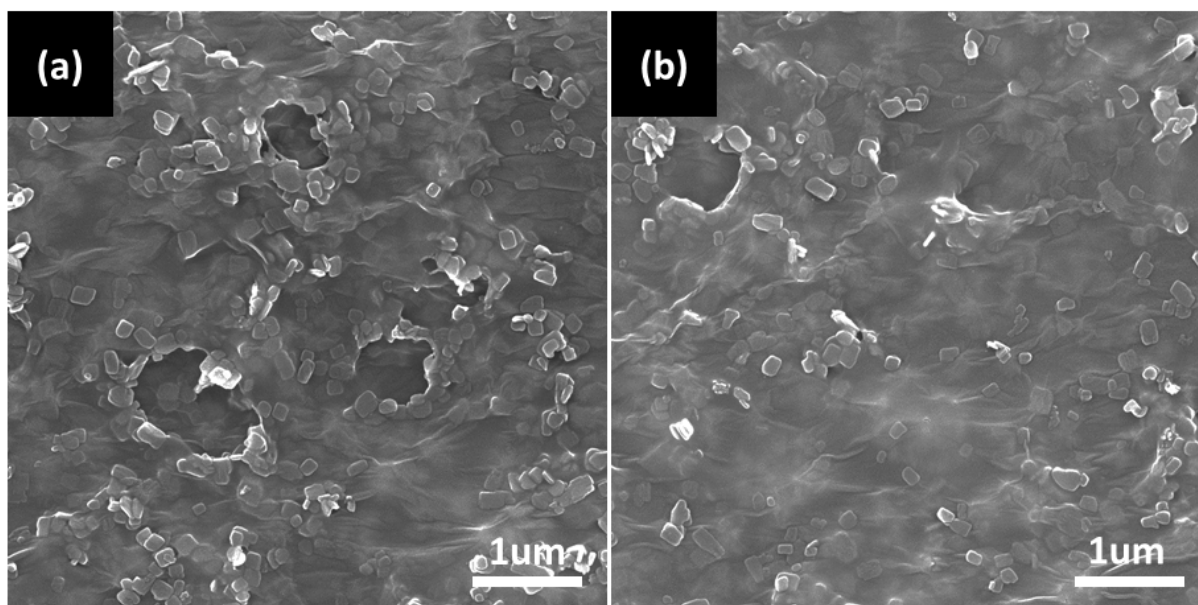


**Fig. S2†** SEM images of LFP@GO, revealing LFP NPs were anchored on GO. With respect to LFP NPs, the presence of crumpled and rough textures on the surfaces of LFP@GO was associated with the flexible and corrugated nature of GO. It should be noted that some exposed GO surface can still be reserved after the electrostatic attraction process between APS-modified LFP NPs and GO. These GO surface will cross-link with the additional GO in the hydrothermal process for the construction of GA.

### S3. Photograph illustration of the synthetic procedure of LFP@N-GA

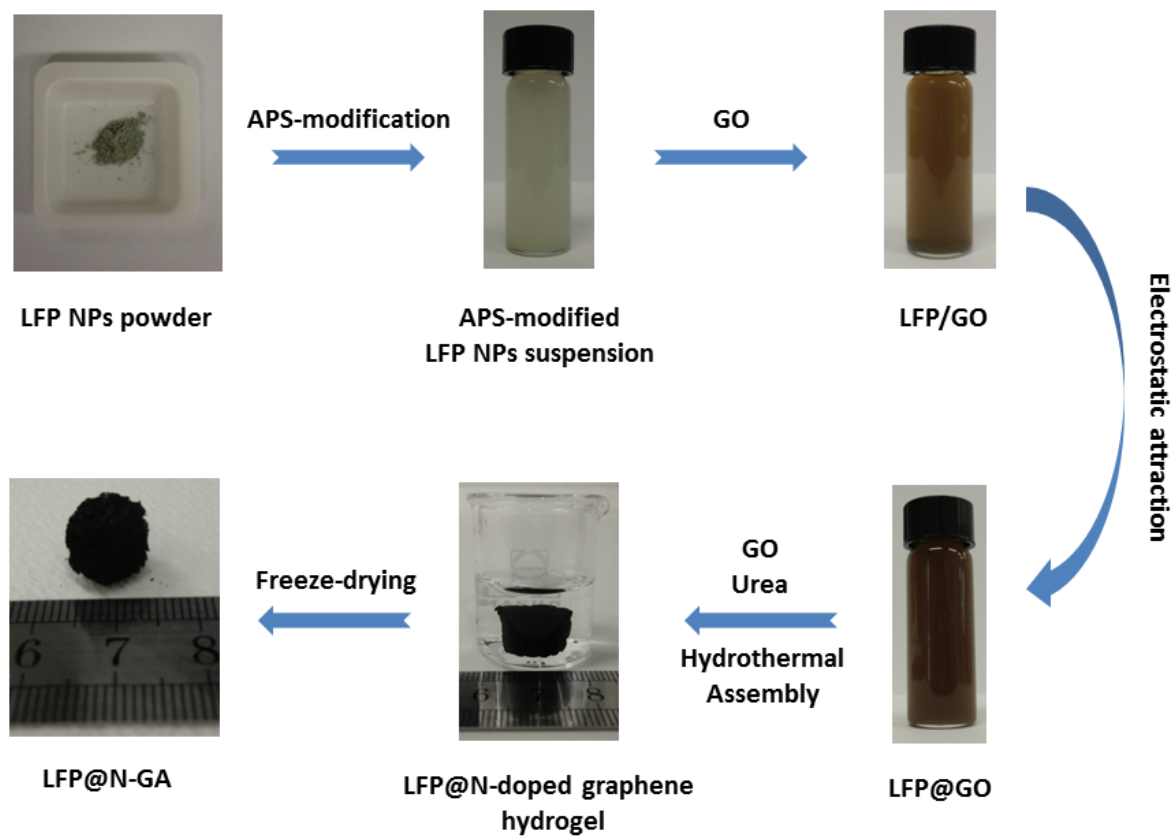


**Fig. S3†** The photograph illustration of the synthetic procedure of LFP@N-GA. It can be seen, through the electrostatic attraction between APS-modified LFP NPs and GO, the obtained LFP@GO suspension was quite uniform and stable. After the hydrothermal process, LFP@GO crossed linked with the additional GO and convert to a hydrogel successfully.

#### S4. Morphology information of LFP@N-GA

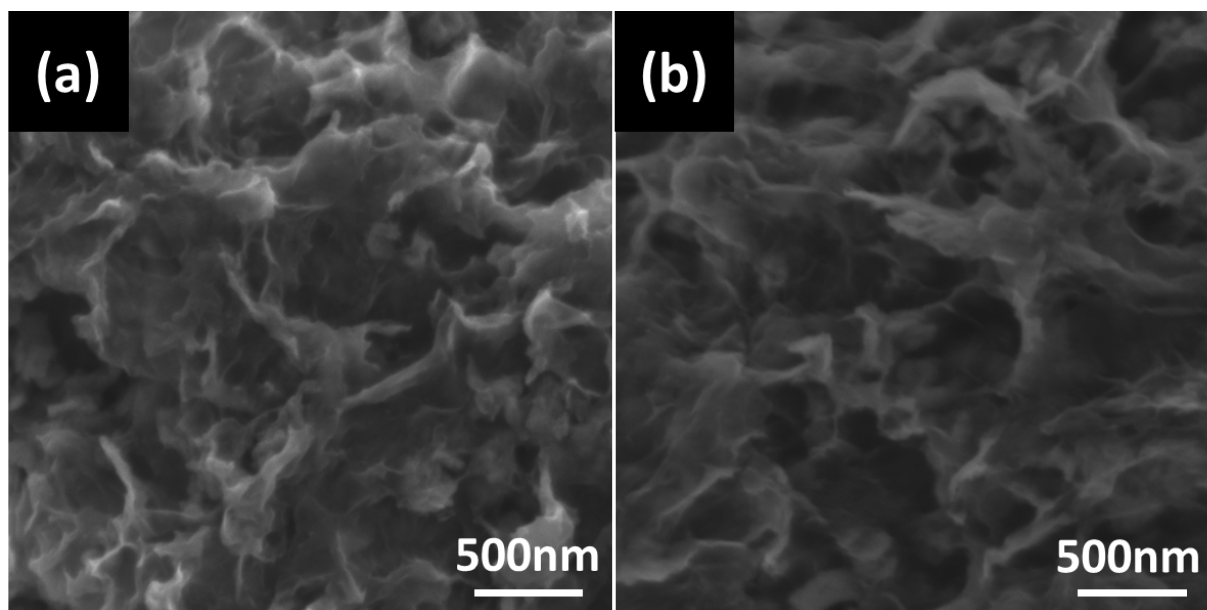


**Fig. S4†** SEM images of LFP@N-GA, showing LFP NPs were embedded within a porous GA.

### S5. Nitrogen isothermal adsorption/desorption measurement of LFP@N-GA, LFP NPs and N-GA

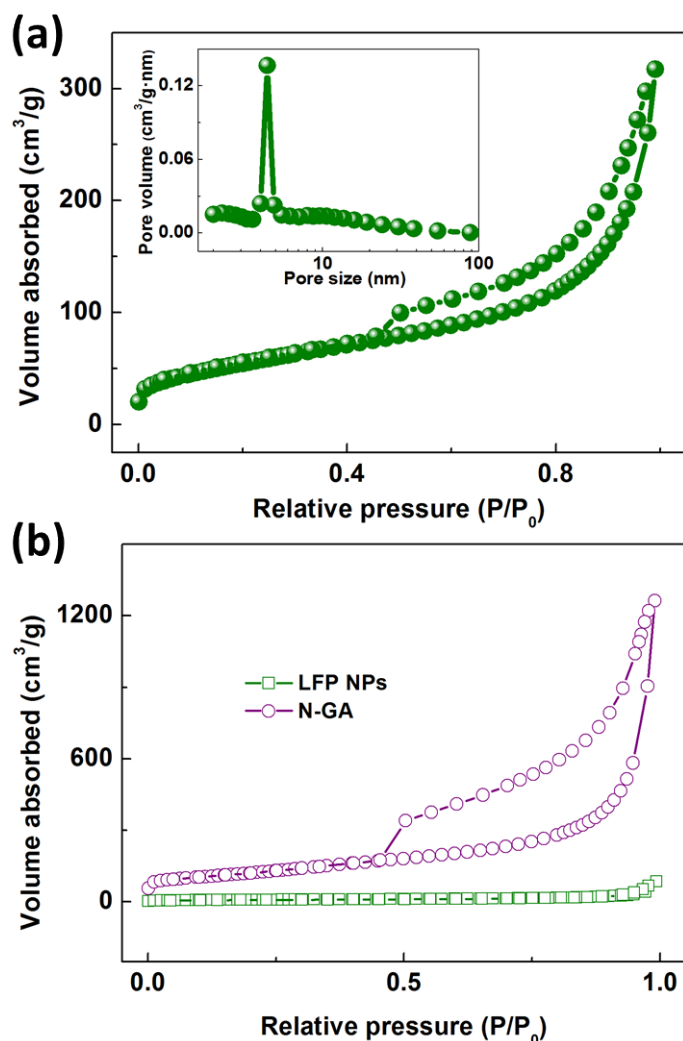


**Fig. S5†** (a) Nitrogen adsorption and desorption isotherm of LFP@N-GA. Inset: The pore-size distribution plot calculated by the BJH formula from the desorption branch isotherm. (b) Nitrogen adsorption and desorption isotherm of LFP NPs and N-GA.

The Brunauer-Emmett-Teller (BET) specific surface area of LFP@N-GA, LFP NPs and N-GA were 199.30, 29.07 and 436.76 m<sup>2</sup>·g<sup>-1</sup>, respectively. The linear combination of the surface area of LFP NPs and N-GA by weight fraction (see Fig. S5†) can be calculated according to Eq. (1):

$$S_c = S_{LFP\ NPs} \times w_{LFP\ NPs} + S_{N-GA} \times w_{N-GA} \quad (1)$$

where  $S_c$  is the calculated linear-combined surface area (m<sup>2</sup>·g<sup>-1</sup>),  $S_{LFP\ NPs}$  is the surface area of LFP NPs (29.07 m<sup>2</sup>·g<sup>-1</sup>),  $w_{LFP\ NPs}$  is the weight fraction of LFP NPs (84.64 wt.%),  $S_{N-GA}$  is the surface area of N-GA (436.76 m<sup>2</sup>·g<sup>-1</sup>), and  $w_{N-GA}$  is the weight fraction of N-GA (15.36 wt.%). The  $S_c$  was calculated to be (91.69 m<sup>2</sup>·g<sup>-1</sup>), which was much lower than the BET surface area of LFP@N-GA, indicative of an alleviative agglomeration between LFP NPs in LFP@N-GA.

### S6. Thermogravimetric analysis of LFP NPs and LFP@N-GA

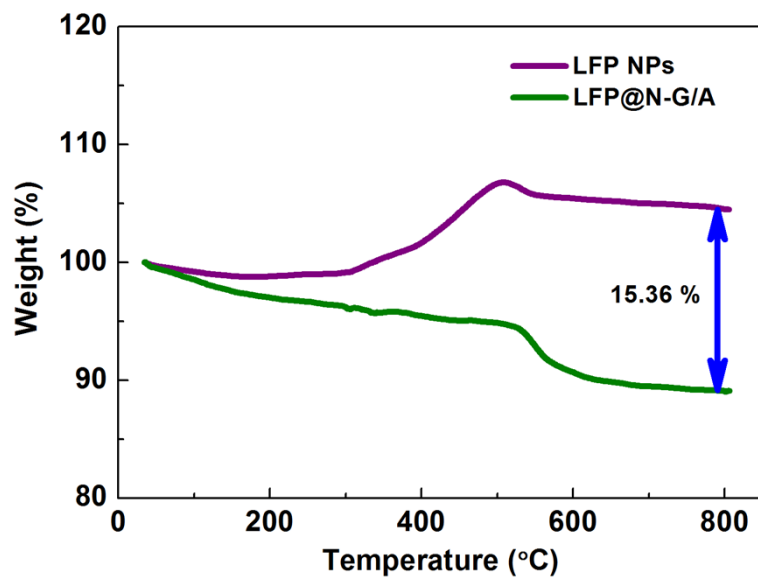


**Fig. S6†** TGA curves of LFP@N-GA of LFP NPs, demonstrated the weight fractions of LFP NPs and N-GA in LFP@N-GA were 84.64 wt.% and 15.36 wt.%, respectively.

### S7. Comparison of the Raman spectra of GO, N-GA and LFP@N-GA

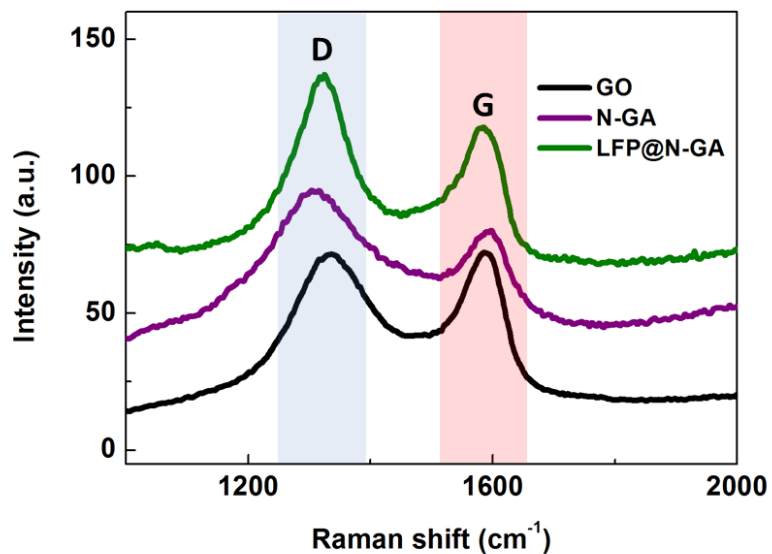


**Fig. S7†** Raman spectra of GO, N-GA and LFP@N-GA. The  $I_D/I_G$  of GO, N-GA and LFP@N-GA were 0.99, 1.30 and 1.33 respectively, suggesting a more disordered structure after N-doping. The shift for both D and G band between N-GA and LFP@N-GA indicated of a charge transfer between N-GA and LFP NPs component in LFP@N-GA.

### S8. Morphology information of commercial LFP/C

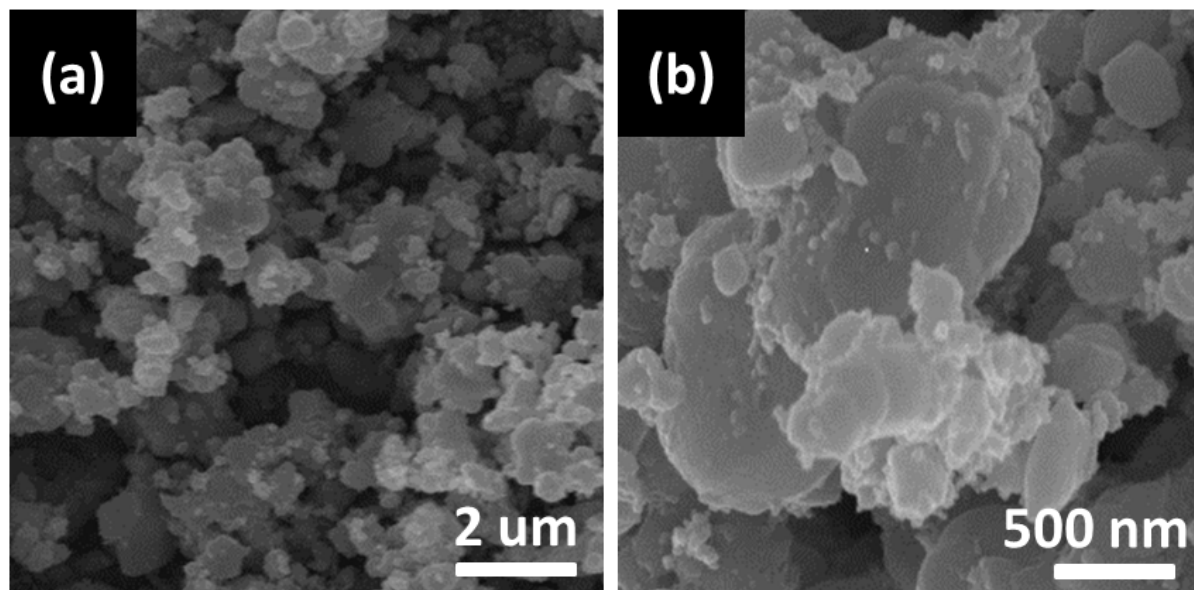


**Fig. S8†** (a) Low- and (b) high-magnification SEM images of commercial LFP/C, revealing that the particles are in irregular in shape with particle size ranging from tens of nm to micrometer. Severe particle agglomeration can also be seen. On contrast to LFP@N-GA, the BET surface area of the commercial LFP/C was measured to be only about  $9.3 \text{ m}^2 \cdot \text{g}^{-1}$  without pores existence.<sup>5</sup>

### S9. Comparison of the middle discharge voltage of commercial LFP/C and LFP@N-GA

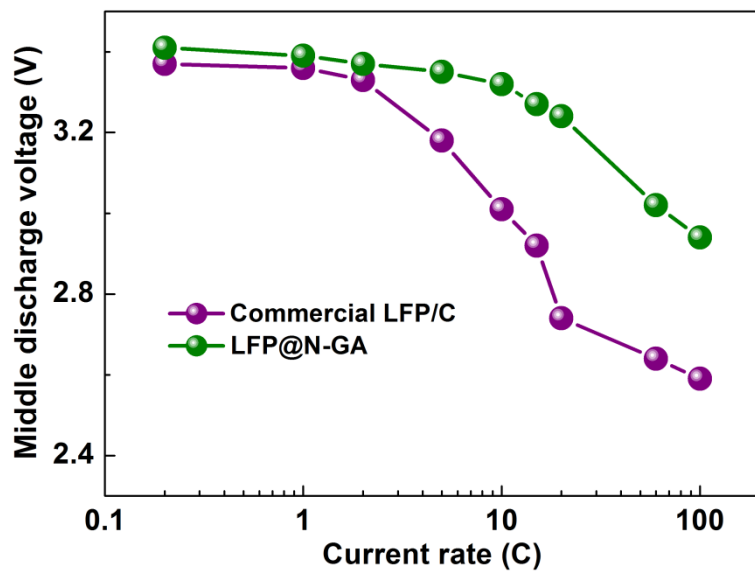


**Fig. S9†** The dependency of the middle discharge voltage on current rate in the range of 0.2 C to 100 C for commercial LFP/C and LFP@N-GA.

### S10. Electrochemical performance of N-GA

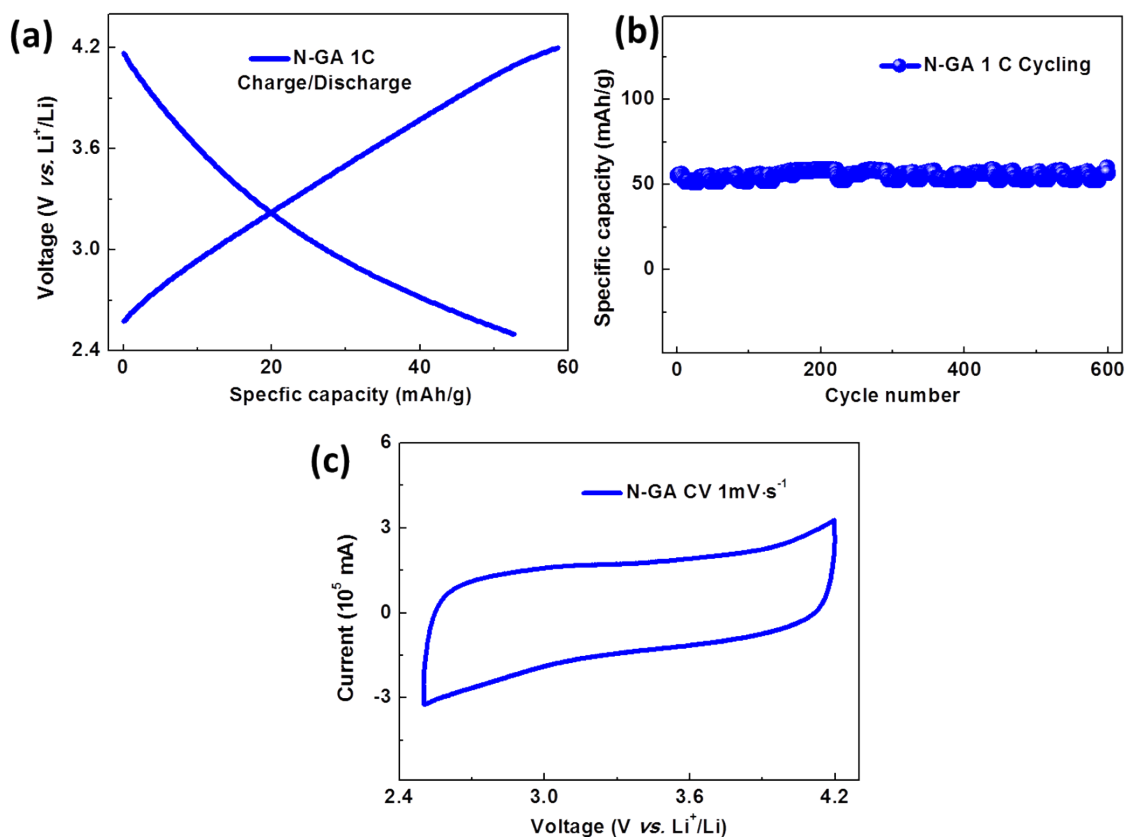


**Fig. S10†** Electrochemical performance of N-GA: (a) Charge/discharge profiles at current rate of 1 C (the current rate is set up based on the nominal capacity of LFP 170 mAh·g<sup>-1</sup>); (b) Cycling performance at 1C and (c) CV profiles at a fixed scan rate of 1 mV·s<sup>-1</sup>. It can be seen N-GA displayed a typical capacitive capacity of 53 mAh·g<sup>-1</sup> (112 F·g<sup>-1</sup>). There was no capacity fading after 600 cycles at this current rate, suggesting a good cycling stability. From the CV curves, it can be seen there were no cathodic/anodic current peaks, indicative of a good electrochemical stability in the chosen electrochemical potential range (2.5 - 4.2 V).

### S11. Morphology information of LFP@N-GA after cycling test

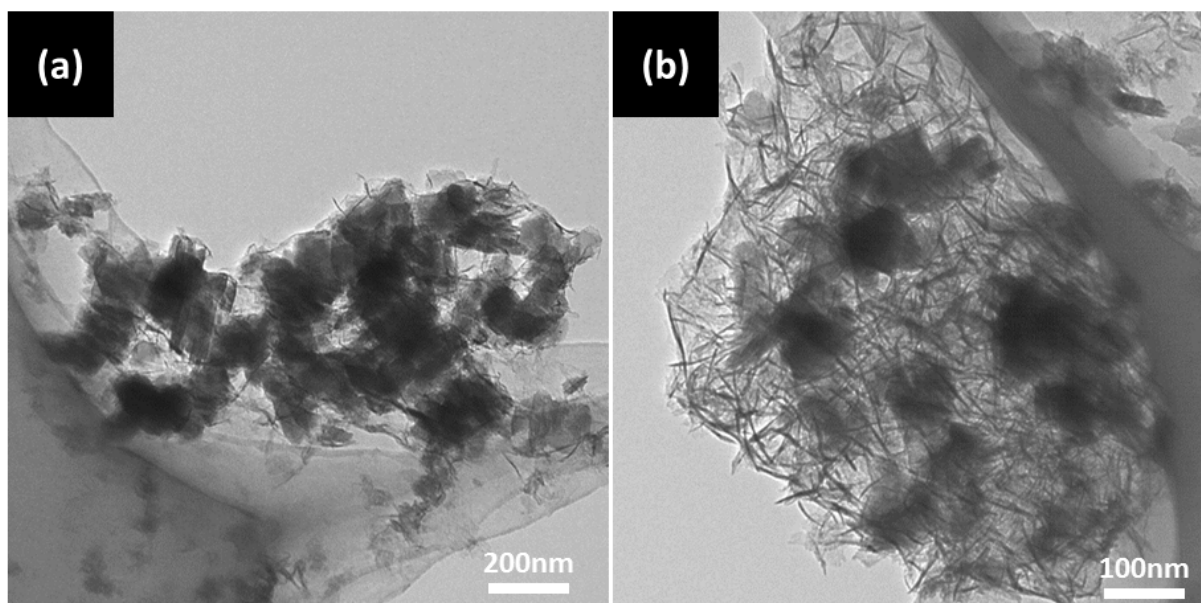


**Fig. S11†** TEM images of LFP@N-GA electrodes after 1000 electrochemical cycles at 10 C, revealing LFP NPs remain well-confined within N-GA after cycling test. The nanoparticles irregularly dispersed around the samples are carbon black, which widely be used as the conductive agent.

### S12. Electrochemical performance of the bare LFP@N-GA electrode

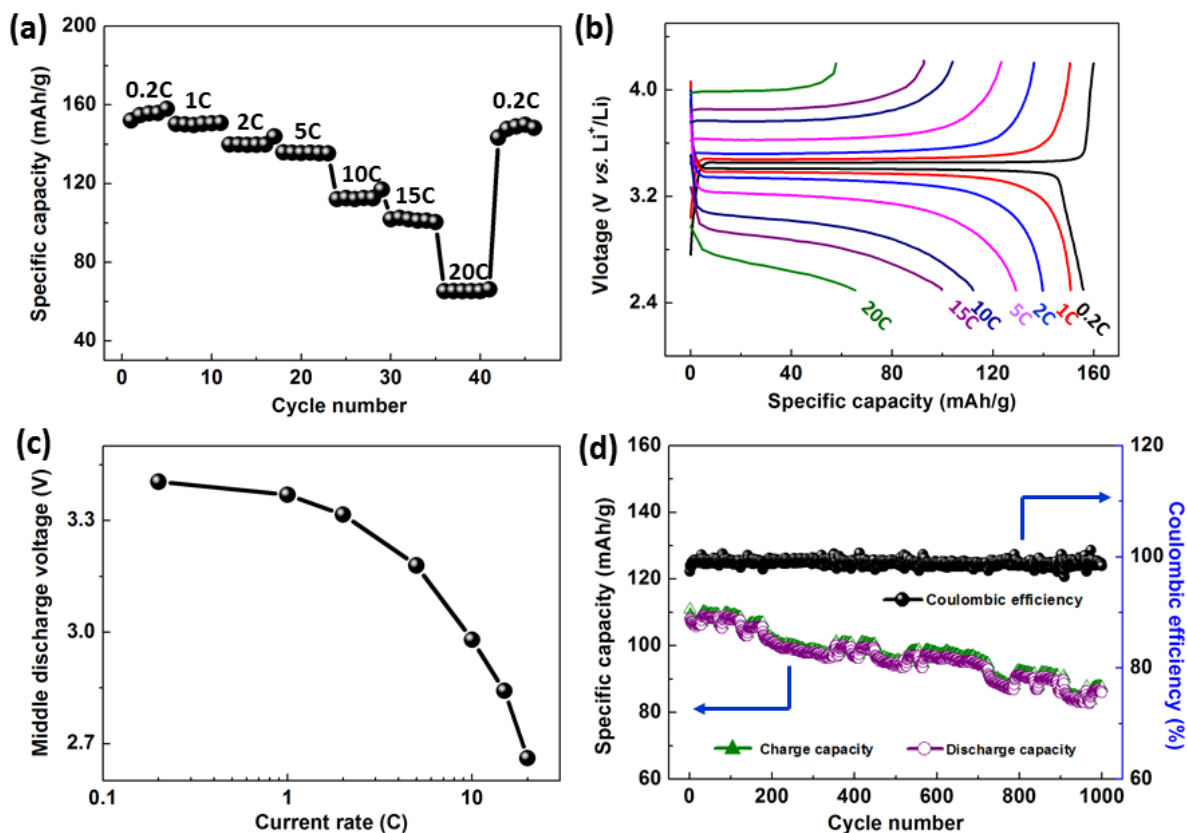


**Fig. S12†** Electrochemical performance of electrode LFP@N-GA (corresponding to 1 layer adhesive tape thicknesses) in the absence of carbon black: (a) Rate capabilities from 0.2 C to 20 C; (b) Charge/discharge profiles at current rate ranging from 0.2C to 20 C; (c) The dependency of the middle discharge voltage on current rate in the range of 0.2 C to 20 C and (d) Cycling performance combined with Coulombic efficiency at 10 C. Such an electrode exhibited discharge capacities of 110 and 66 mAh·g<sup>-1</sup> at 10 and 20 C, respectively. The reversible capacity of bare LFP@N-GA electrode sustained 86 mAh·g<sup>-1</sup> after 1000 cycles at 10 C with a capacity retention of 80%. Although the electrochemical performance of the carbon black-free LFP@N-GA electrode was poorer than that of the electrode with carbon black, it was still superior to commercial LFP/C (with the addition of carbon black).

### S13. Electrochemical performance of LFP@N-GA and commercial LFP/C electrode with different mass loading

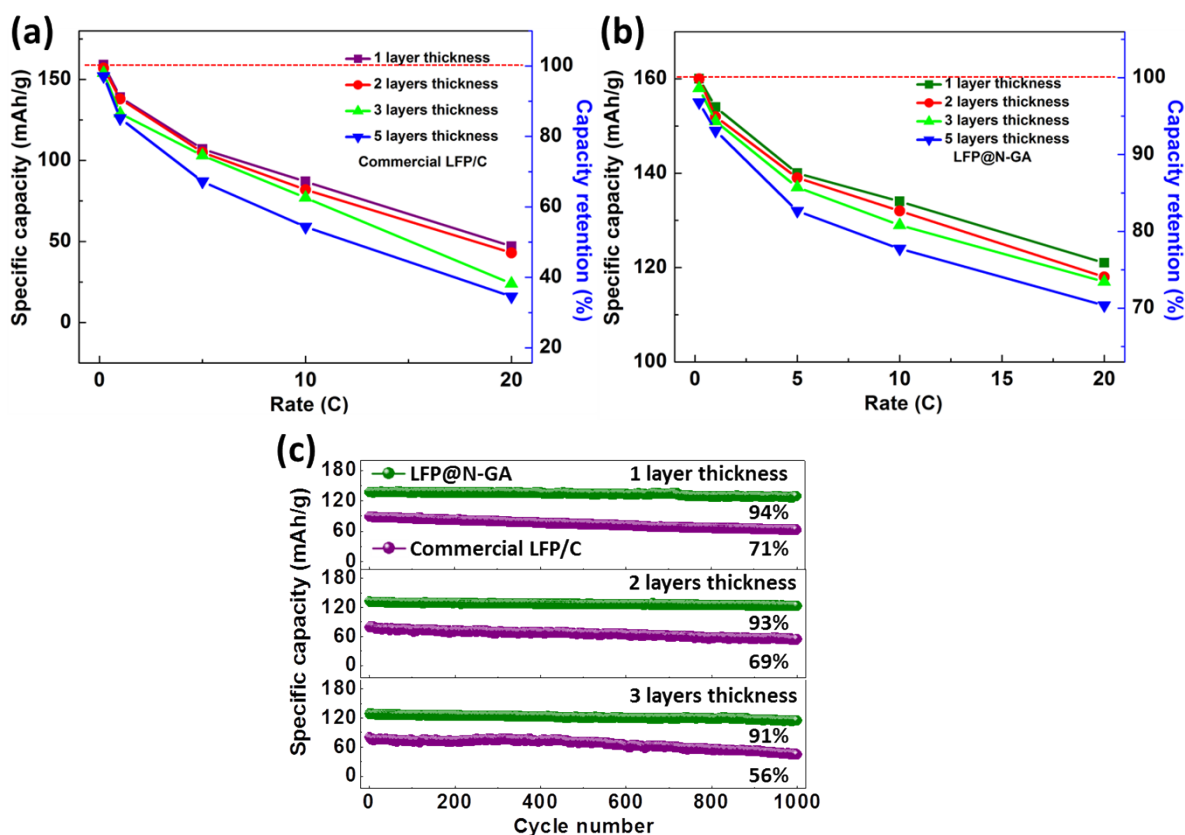


**Fig. S13†** Electrochemical performance of LFP@N-GA and commercial LFP/C electrode with different mass loading: (a, b) rate performance and (c) cycling stability at 10C. It can be seen the capacity and cycling stability of commercial LFP/C decayed rapidly with the increase in loading mass due to increased polarization, especially along the direction perpendicular to the current collector. While for LFP@N-GA, the capacity retention and cycling stability were still much better than commercial LFP/C, suggesting the inside 3D bicontinuous conductive network effectively facilitate both  $\text{Li}^+$  and electron transport kinetics, and thus, reducing the polarization.

#### S14. Li<sup>+</sup> diffusion coefficient during charge/discharge

Randles-Sevcik equation,<sup>5</sup> which is always used to calculate the Li<sup>+</sup> diffusion coefficient during charge/discharge, is represented in Eq. (2):

$$I_p = 2.69 \times 10^5 n^{3/2} A C_0 D_{Li}^{1/2} \nu^{1/2} \quad (2)$$

where  $I_p$  is the peak current (A),  $n$  is the number of electrons transferred per molecule during the electrochemical reaction (for LFP,  $n = 1$ ),  $A$  is the active surface area of the electrode (cm<sup>2</sup>),  $C_0$  is the molar concentration of Li<sup>+</sup> in LFP ( $2.28 \times 10^{-2}$  mol·cm<sup>-3</sup>),  $D_{Li}$  is the Li<sup>+</sup> diffusion coefficient in LFP (cm<sup>2</sup>·s<sup>-1</sup>), and  $\nu$  is the scanning rate (V·s<sup>-1</sup>). According to this formula,  $D_{Li}$  is proportional to  $I_p^{-1/2}$ .

**S15. Comparison of the rate capability of LFP@N-GA with previously reported 2D graphene-modified LFP composites and 3D porous LFP/carbon composites**

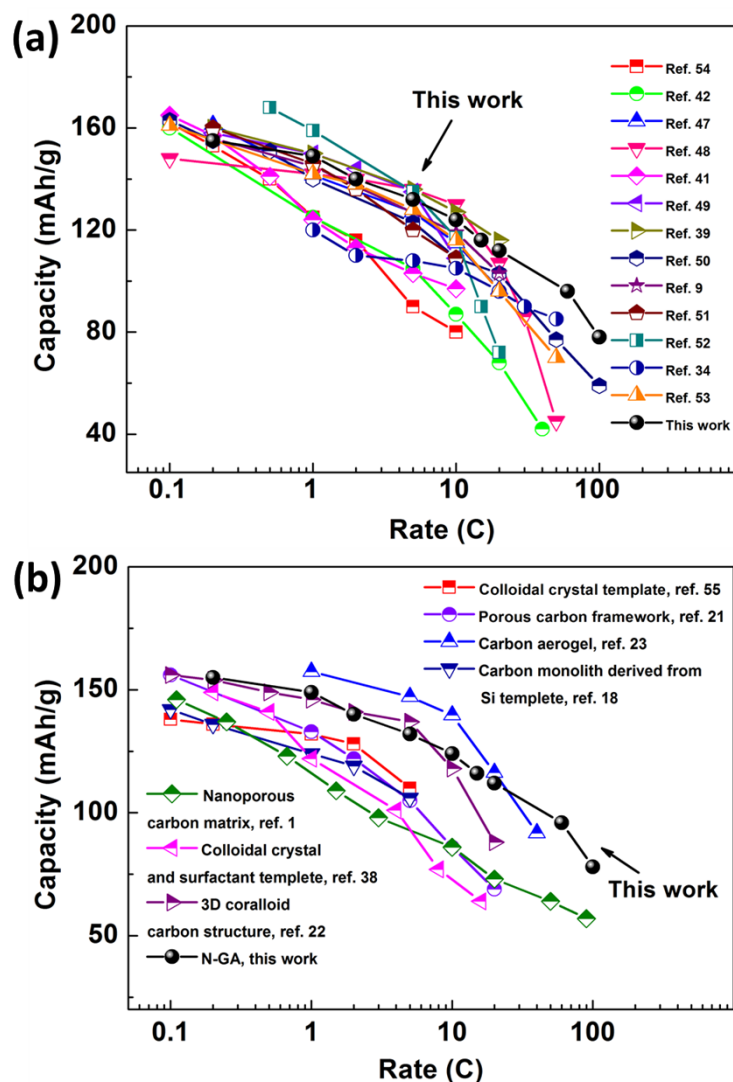


**Fig. S14†** Comparison of the rate capability of LFP@N-GA with previously reported 2D graphene-modified LFP composites (a) and 3D porous LFP/carbon composites (b).

### S16. The extension of the preparation method

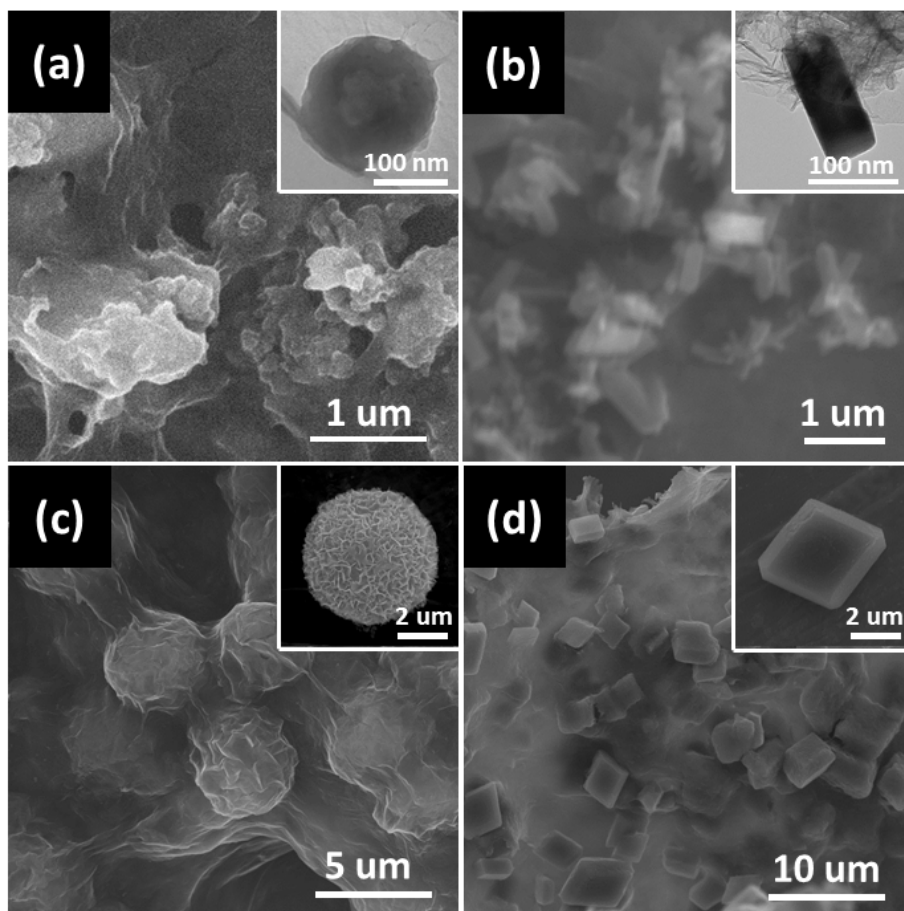


**Fig. S15†** The extension of the preparation method to other LFP materials with different morphologies: (a) SEM and TEM (inset) image showing the nanoparticle morphology of LFP component; (b) SEM and TEM (inset) image revealing the nanorod morphology of LFP component; (c) SEM images showing the hierarchical microsphere morphology of LFP component, and (d) SEM images revealing the microrhomb morphology of LFP component. Moreover, the method can be easily transferred to other electrochemical active materials, such as  $\text{LiMn}_2\text{O}_4$ ,  $\text{SnO}_2$  and  $\text{SiO}$  etc., which is being carried out.

1. Z. Xiong, L. L. Zhang, J. Ma and X. S. Zhao, *Chem. Commun.*, 2010, **46**, 6099-6101.
2. L. Wang, X. He, W. Sun, J. Wang, Y. Li and S. Fan, *Nano Lett.*, 2012, **12**, 5632-5636.
3. W.-B. Luo, S.-L. Chou, Y.-C. Zhai and H.-K. Liu, *J. Mater. Chem. A*, 2014, **2**, 4927-4931.
4. W. Wei, S. Yang, H. Zhou, I. Lieberwirth, X. Feng and K. Müllen, *Adv. Mater.*, 2013, **25**, 2909-2914.
5. B. Wang, Q. Wang, B. Xu, T. Liu, D. Wang and G. Zhao, *RSC Adv.*, 2013, **3**, 20024-20033.